Lifetime Analysis of Motorized Spindle Bearings Based on Dynamic Model

Jun Ying
  College of Mechanical Science and Engineering

Zhaojun Yang
  College of Mechanical Science and Engineering

Chuanhai Chen (✉ cchchina@foxmail.com)
  College of Mechanical Science and Engineering

Guoxiang Yao
  College of Mechanical Science and Engineering

Wei Hu
  College of Mechanical Science and Engineering

Hailong Tian
  College of Mechanical Science and Engineering

Research Article

Lifetime analysis of motorized spindle bearings based on dynamic model

Jun Ying[1,2], Zhaojun Yang[1,2], Chuanhai Chen[1,2*], Guoxiang Yao[1,2], Wei Hu[1,2], Hailong Tian[1,2]

Abstract The traditional probabilistic-based lifetime evaluation methods for motorized spindles neglect the effects of load dynamic and structure difference. Hence, a dynamic-model-based lifetime estimation method combining these effects is proposed to improve the estimating results for motorized spindles, especially in the design stage. Considering the bearings lifetime has dramatically influenced the reliability of motorized spindles, this paper establishes a shaft-bearing-toolholder based on a dynamic model to estimate the bearing group lifetime. The proposed dynamic model is closer to the actual structure in spindles, indicating the stiffness of bearings and contact surface conditional on the inputting radial-and-axial forces is nonlinear. The stiffness model is verified by finite element analysis and experiment. The load applied to bearings is accurately calculated through the dynamic model. Then, the load is introduced to a well-known bearing lifetime model, thereby calculating the lifetime of each bearing and its group. The bearing lifetime results under different conditions of preload, clamping force, and cutting force are discussed.

Keyword Lifetime, Dynamics model, Motorized spindle bearings, Contact surface, Dynamic cutting force.

✉ Chuanhai Chen
cchchina@foxmail.com

1   Key Laboratory of CNC Equipment Reliability, Ministry of Education, Jilin University, Changchun, Jilin, 130025, China
2   School of Mechanical and Aerospace Engineering, Jilin University, Changchun 130025, China

1 Introduction

As the key part of the machine tool, the performance of the motorized spindle greatly influences the high quality and efficient production of CNC machine tool[1, 2]. Due to the infrequent failures and slow performance degradation processes, obtaining enough data to evaluate motorized spindle lifetime is time-consuming. Moreover, the different structures and operation loads result in the significant heterogeneity of motorized spindles, indicating the estimation of the individual lifetime is highly required. It is known that the bearing plays a crucial role in the motorized spindle system, whose failures cover a large proportion of the system failures[3, 4]. Hence, to improve the reliability of motorized spindles in the design stage[5], an accurate and efficient lifetime evaluation for bearings considering the difference of applied load is very important.

The lifetime of machine tools and their components are commonly described using probabilistic models[6]. However, the estimation accuracy of these models depends on the number of fault data whose collection is time-consuming for long-life systems or components. To improve the estimation accuracy, Yang[7] and Peng[8] et al. proposed the small sample size method to relieve the demand for many data. To get a more accurate model considered the other factors, Yang[9] and Mu[10] considered the influence of load conditions on the reliability of spindle and machine tools. Some scholars proposed to use prior information and observation data to establish the degradation model for the spindle failure. Peng[11] analyzed the degradation of the spindle with Bayesian method under time-varying degradation rates. Guo[12] proposed a Bayesian information fusion method to

model the degradation process of the heavy-duty machine tool's spindle from multiple sources. Both statistical models and degenerate models use many prior data to eliminate the influence of external factors on homogeneous structures. But for the very different structures, it may give inexact or misleading results to the products. It is known that through different structures transmission, the load applied to the component can be different even if the input force and component are the same. The load difference can cause a change of components' lifetime and thereby impact the system's reliability. Moreover, the input force is dynamic during spindles' operation, indicating that the load applied to the components is also dynamic. The dynamic load makes its relationship with component lifetime more complicated.

To better estimate the lifetime of long-lifetime products having different structures and dynamic forces, dynamics-based lifetime estimation methods have been proposed. The dynamic model considers the system's structure and can calculate the dynamic load applied to components accurately. An accurate load result is very useful for lifetime estimation. Another advantage of dynamic-based lifetime estimation methods is the independence from lifetime data, helping to quickly evaluate the reliability of new products in the design period. Fu et al.[13] analyzed the fatigue damage of flange and bolt on the wind turbine tower with the vibration response. Nejad et al.[14] analyzed the long-term fatigue damage for gear tooth root bending in the wind turbine's drivetrains with dynamics. Cheng et al.[15] introduced a wear model for the ball screw mechanism considering dynamic fluctuations loading. For the motorized spindle system, Li et al.[16] used the dynamic load to calculate the lifetime of the shaft on the motorized spindle but neglects the influence of joint surface structure on load. Zhang [17] analyzed the influence of the preload and angular deviation of bearing on the spindle system lifetime according to the dynamics model. However, the paper only studied the static load effect on a simple structure that did not consider the toolholder. The lifetime analysis for motorized spindles considering the shaft-bearing-toolholder structure and dynamic load has not been relatively complete conducted to the best of our knowledge.

In this paper, according to the structural characteristics of the motorized spindle, the multiple degrees dynamic model of the shaft-bearing-toolholder structure is established based on rotor dynamics. The influence of axial and radial forces on bearing stiffness and contact surface stiffness is integrated into the proposed model. The dynamic response of each bearing in the motorized spindle is analyzed under the different conditions of preloads, cutting force, and clamping forces.

The rest of this article is organized as follows. Section 2 establishes the dynamic model for the shaft-bearing-toolholder structure in the motorized spindle. In Section 3, the lifetime method of the bearing group in the motorized spindle is presented using the dynamic model. In Section 4, the stiffness in the dynamic model is verified by the experiment. In Section 5, the lifetime of each bearing and its groups are compared under different conditions of bearing stiffness, clamping force, and rotating speed. Some concluding remarks are made in Section 6.

2 Dynamic model of motorized spindle

The internal structure model of the motorized spindle is shown in Fig. 1. Due to the shaft
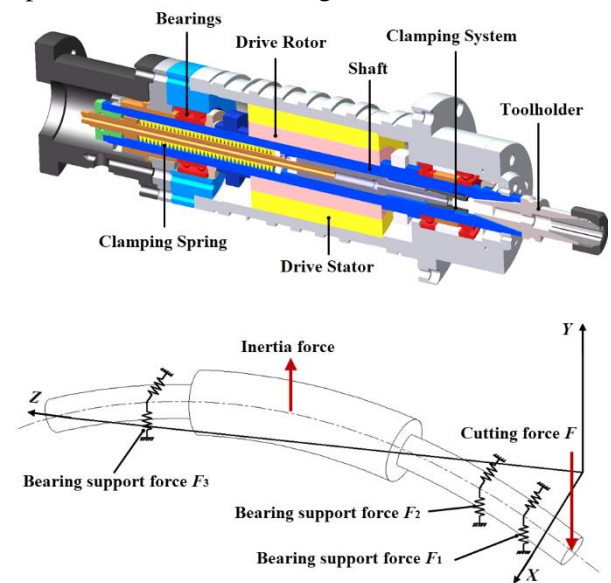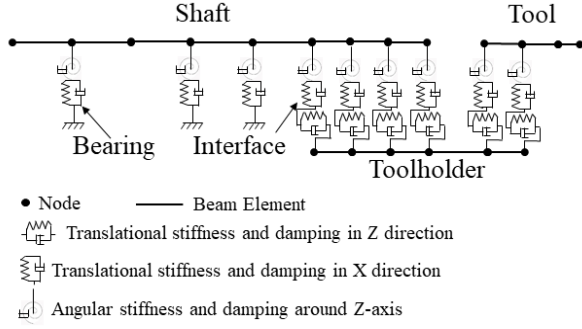

Fig. 1 The motorized spindle system

Fig. 2 Finite element model for the spindle-bearing system

deflection, gyroscopic moment, and bearing stiffness's nonlinearity, the bearing load motivated by cutting force is dynamic and nonlinear in different positions. Hence the response of bearings in different positions is also different. Therefore, the simplified dynamic model of the motorized spindle should be established to determine this relationship between the cutting forces and the loads on the bearings.

According to the internal structure of the motorized spindle, the motorized spindle can be simplified into three parts: shaft, bearing, and toolholder. In this section, a shaft-bearing-toolholder dynamic model is established considering the interaction among them.

2.1 Dynamic model establishment

The most common methods to establish a rotor dynamics model include the finite element and transfer matrix methods[18, 19]. This paper uses the Timoshenko beam element in the finite element method to model the dynamics.

The dynamic model of the shaft-bearing-toolholder system is shown in Fig. 2. The model contains two front bearings and two rear bearings. The preload is added to bearings to ensure adequate support stiffness. The contact surface matches the toolholder and shaft through the clamping force. Following this, the vibration characteristics of the whole shaft-bearing-toolholder system can be obtained when applying the cutting force to the end of the toolholder.

According to Timoshenko beam theory, the finite element model of spindle-bearing is established by

$$[M]\{\ddot{q}\}+[C]\{\dot{q}\}+\Omega[G]\{\dot{q}\}+\left([K_b]+[K_C]+[K]\right)\{q\}=\{F\}, \tag{1}$$

where $[M]$ is the mass matrix, $[C]$ is the damping matrix, $[G]$ is the Gyro moment matrix, Ω is the velocity of spindle rotation angular, $[K]$ is the stiffness matrix for the shaft, $\{q\}$ is the generalized displacement, $[K_b]$ is the stiffness matrix of bearings, $[K_C]$ is the contact stiffness matrix of the spindle contact surface and the toolholder contact surface, $\{F\}$ is the vector of cutting force, including distributed force and concentrated force.

The stiffness matrix of bearing $[K_b]$ and the contact stiffness matrix $[K_C]$ are the spindle support and components connection parameters, which need to be established additionally. Usually, the tooltip frequency response test is used to identify the bearing stiffness and contact stiffness, which relies on the detection equipment, and the spindle with different structures needs to be measured again[20-23]. To avoid this limitation and facilitate the prediction of spindle dynamic performance in the design phase, this paper uses the physical model to establish the bearing and contact stiffness. It is known that the physical model has a better accuracy of the bearing stiffness $[K_b]$ estimation. Based on the Hertz contact theory quasi-static model, the five freedom analysis method is used to obtain the load distribution and bearing deflection under any working conditions[24].
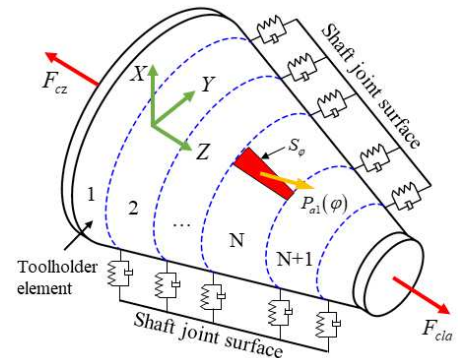

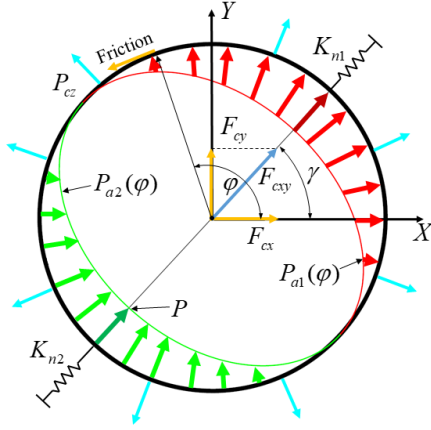Fig. 3 The model of toolholder under clamping and axial force

Fig. 4 Force analysis of the element under the radial force

The contact stiffness $[K_C]$ is the elastic connection between toolholder and shaft, which is the weak point in the spindle system. It can influence the stiffness of the whole spindle system. YOSHIMURA[25] proposed a physical model to model the relationship between contact pressure and contact stiffness. Recently, this relationship model has been developed by considering many factors' influence on the contact stiffness, such as the stress distribution and centrifugal force[26], the roughness[27]. However, the dynamic load is seldom considered, including radial force and axial force on the joint surface. But in practice, during the spindle rotation, the cutting force is dynamically alternating and amplitude fluctuation. The dynamic axial and radial force on the spindle will constantly change the contact surface's stress distribution, thereby changing the contact stiffness. Since damping in the system will limit the amplitude of the instantaneous load, considering the static load as the only interest will give inaccurate prediction results, which cannot reflect the actual load

condition. Hence, it is necessary to analyze the influence of the dynamic load on the contact stiffness.

2.2 The contact stiffness considering dynamic force

This subsection formulates the dynamic contact stiffness on the toolholder under the condition of dynamic axial-and-radial force.

Initially, assume the spindle-toolhodler does not have any manufacturing error. As shown in Fig. 3, the toolholder is divided into N elements, and one of the elements subjected to the radial force F_{cx}, F_{cy}, and the axial force F_{cz}. Under the action of axial force F_{cz}, the contact pressure of the contact surface is given by

$$P_{cz} = \frac{F_{cla} - F_{cz}}{S_c\left(\sin\theta_t + \mu_t\cos\theta_t\right)}, \qquad (2)$$

where F_{cla} is the clamping force, S_c is the area of the element contact surface, θ_t is the taper angle of the toolholder, μ_t is the friction coefficient.

The cross-section of the contact surface element is shown in Fig. 4. The resultant radial force F_{cxy} on the one element of the contact surface is produced by the radial force F_{cx} and F_{cy} in the directions X and Y. The angle between F_{cxy} and the X is γ. Under radial force F_{cxy}, the contact pressure on the one side would increase while the other side would decrease. Consider the contact pressure acting by the radial force on the contact surface as a cosine function distribution[28]. Then, the increasing contact pressure $P_{a1}(\varphi)$ and the decreasing contact pressure $P_{a2}(\varphi)$ dependent on the angle φ are

$$\begin{cases} P_{a1}(\varphi) = P\cos(\varphi - \gamma) & (\gamma - \pi/2 \le \varphi < \gamma + \pi/2) \\ P_{a2}(\varphi) = P\cos(\varphi - \pi - \gamma) & (\gamma + \pi/2 \le \varphi < \gamma + 3\pi/2) \end{cases}, \qquad (3)$$

where P is the maximum contact pressure of the change pressure distribution.

Therefore, the rule of pressure change generated by the radial force F_{cx} and F_{cy} along the angle φ follows

$$\begin{cases} P_{b1}(\varphi) = P_{cz} + P_{a1}(\varphi) \\ P_{b2}(\varphi) = P_{cz} - P_{a2}(\varphi) \end{cases}, \qquad (4)$$

if $P_{a2}(\varphi) \ge P_{cz}$, the contact surface in this angle lost contact. No pressure is generated, and the contact stiffness equals 0. When the contact pressure on one side disappears completely, the contact stiffness only exists on the other side

After the change of contact pressure, the force equation in γ direction is

4

$$\begin{cases} F_{\gamma 1} = \int_{\gamma-\frac{\pi}{2}}^{\gamma+\frac{\pi}{2}} P_{b1}(\varphi) S\varphi\cos(\varphi-\gamma)d\varphi + 2\int_{\gamma+\frac{\pi}{2}}^{\gamma+\pi} \mu P_{b1}(\varphi) S\varphi\sin(\varphi-\pi-\gamma)d\varphi \\ F_{\gamma 2} = \int_{\gamma-\frac{\pi}{2}}^{\gamma+\frac{\pi}{2}} P_{b2}(\varphi) S\varphi\cos(\varphi-\gamma)d\varphi + 2\int_{\gamma+\frac{\pi}{2}}^{\gamma+\pi} \mu P_{b2}(\varphi) S\varphi\sin(\varphi-\pi-\gamma)d\varphi \end{cases}, \tag{5}$$

where S_φ is the cone area per unit angle, μ is the friction coefficient.

The equilibrium equation under the resultant force F_{cxy} is

$$F_{\gamma 1} - F_{\gamma 2} = F_{cxy} . \tag{6}$$

According to Eq.(6), the maximum contact pressure P can be obtained. Therefore, the change of

$$\begin{cases} K_{inx} = \int_{\gamma-\frac{\pi}{2}}^{\gamma+\frac{\pi}{2}} K_{n1}(\varphi) S_\varphi |\cos\varphi| d\varphi + \int_{\gamma+\frac{\pi}{2}}^{\gamma+\frac{3}{2}\pi} K_{n2}(\varphi) S_\varphi |\cos\varphi| d\varphi \\ K_{iny} = \int_{\gamma-\frac{\pi}{2}}^{\gamma+\frac{\pi}{2}} K_{n1}(\varphi) S_\varphi |\sin\varphi| d\varphi + \int_{\gamma+\frac{\pi}{2}}^{\gamma+\frac{3}{2}\pi} K_{n2}(\varphi) S_\varphi |\sin\varphi| d\varphi \end{cases}, \tag{8}$$

The contact stiffness between the two nodes in the dynamic model can be expressed by

$$[K_C] = \begin{bmatrix} k_{inx} & & & -k_{inx} & & \\ & k_{iny} & & & -k_{iny} & \\ & & 0 & & & 0 \\ & & & 0 & & & 0 \\ -k_{inx} & & & k_{inx} & & \\ & -k_{iny} & & & k_{iny} & \\ & & 0 & & & 0 \\ & & & 0 & & & 0 \end{bmatrix} \tag{9}$$

The complete toolholder model should include the contact stiffness of toolholder-shaft and toolholder-tool. Because the modeling method of toolholder-tool is similar to toolholder-spindle, the modeling process of toolholder-tool is not given in the paper.

3 Lifetime evaluation of spindle bearings

The cutting force is the key load that affects the lifetime of the motorized spindle. A typical cutting force $\{F\}$ is selected as the external excitation in the dynamic model of the spindle to realize bearing lifetime evaluation. The node time history displacement of the bearing $\{q_b\}$ can be extracted from $\{q\}$ by substituting the cutting force $\{F\}$ into Eq.(1). Then, the time history load F_b of each bearing in the spindle equals the multiplication of

unit contact stiffness on the contact surface [25] is

$$\begin{cases} K_{n1}(\varphi) = \alpha(P_{b1})^\beta \\ K_{n2}(\varphi) = \alpha(P_{b2})^\beta \end{cases}, \tag{7}$$

where α and β are constant parameters dependent on the surface material properties.

So, the contact stiffness of the contact surface is the sum of the normal contact stiffness along the X-axis and Y-axis, given by

the bearing stiffness matrix $[K_b]$ and the time history displacement $\{q_b\}$ as

$$F_b = [K_b] * \{q_b\} . \tag{10}$$

The load F_b is a time series with variable amplitude load, which can be changed into constant amplitude cyclic load by rain flow calculation. Then, the two-dimensional data of bearing forces are obtained with different amplitudes and average values. According to the principle of the bearing force, the maximum load of each cutting force cycle is taken as the applied radial load F_r of the bearing. Because the preload of the bearing also has a significant impact on the bearing lifetime, the resultant force F_0 is the sum of the preload force and the axial force in the cutting force. The equivalent dynamic load F_m of the bearing is calculated as follows.

$$F_m = X_b F_r + Y_b F_0 , \tag{11}$$

when $F_0/F_r \leq e$, $X_b=1$. When $F_0/F_r \leq e$, X_b is the rotation factor, and Y_b is the thrust factor of the bearing.

According to the Palmgren-Miner rule, the equivalent dynamic load F_m in cyclic load considering preload is transformed into the average

5

payload P_m, that is

$$P_m = \left(\frac{1}{N} \int_0^N F_m^p dN \right)^{\frac{1}{p}}, \qquad (12)$$

where N is a total number of cycles.

For the ball bearing $p=3$, the lifetime of the single bearing under the specific cutting force according to the calculation method of bearing lifetime[29] is

$$L_h = a_1 a_2 a_3 \frac{10^6}{60n} \left(\frac{C_r}{P_m} \right)^3, \qquad (13)$$

where a_1 is the lifetime parameter, a_2 is the lifetime coefficient of the bearing characteristics, a_3 is the lifetime coefficient of the working condition, n is the rotating speed, and C_r is the rating radial load of the bearing.

Consider the life of other parts in the motorized spindle is infinite. The lifetime of the bearing group is close to that of the motorized spindle. Therefore, there is

$$\frac{1}{L^e} = \frac{1}{L_1^e} + \frac{1}{L_2^e} + \cdots + \frac{1}{L_h^e}, \qquad (14)$$

where $e=1.1$ and h is the number of bearings in the motorized spindle

4 Dynamic model verification

The contact stiffness model is verified by the finite element analysis of the stress distribution of the cone element, and the static stiffness model of the motorized spindle is verified by the impact test and load experimental.

4.1 Stress distribution on the contact element

The contact surface of toolholder is divided into several elements, and the stress distribution of one element is analyzed. The small end diameter of the element is 20mm, the taper of the toolholder is 7/24, the clamping force on the element is 80N, the friction coefficient is 0.1 for the contact surface. In the calculation, the radial forces are from 0 to 80N.

The von Mises' contact pressure under the radial force is illustrated in Fig. 5, where the contact pressure is biased to one side. The pressure

increases on one side of the toolholder unit by increasing radial force, while the pressure on the other side decreases. The center of the tool holder is shifted to the loading direction, which results in the uneven distribution of contact pressure on both sides. On the pressure-increasing side, the error between the theoretical value and the simulation value is small. In contrast, the error on the pressure decreasing side is large, but the overall trend is the same.

The change of contact stiffness under radial force is shown in Fig. 6. The contact stiffness increases linearly with the increasing radial force of the contact element. The phenomenon is that the radial force changes the contact pressure distribution of the contact surface, and the contact stiffness increases sharply on the contact pressure increasing side. Because the effect of axial load in cutting force on the toolholder is only to increase or decrease the clamping force in proportion, the influence of axial force is not discussed in this paper.
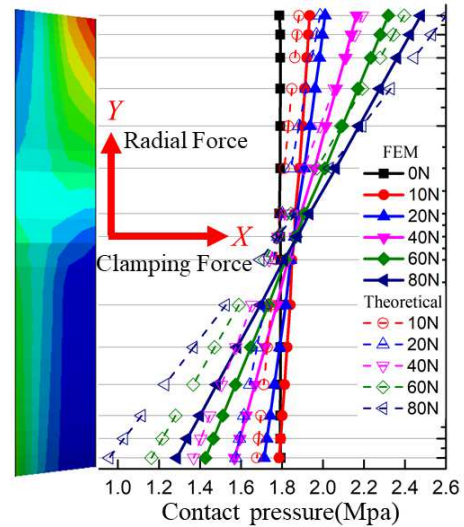

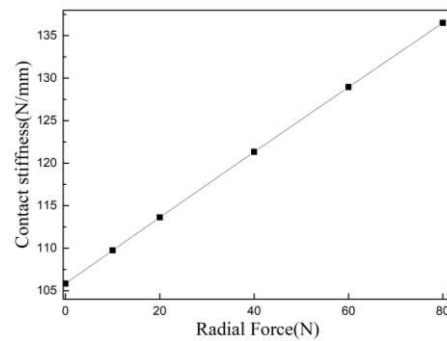Fig. 5 The contact pressure distribution of toolholder unit

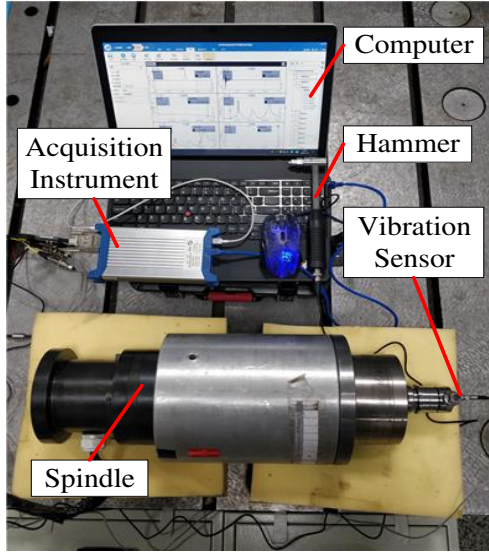Fig. 6 Contact stiffness under radial force

6

Fig. 7 Experimental setup for the spindle

4.2 Verification of stiffness model of motorized spindle

In order to verify the dynamic model of the motorized spindle, the impact test was done on the motorized spindle that assembled the tool and test rod. The model of the motorized spindle is JSZD105C produced by SHANGDONG BEAT PRECISION. The shaft is supported by four bearings which are angular contact ball bearing under the preload 280N. The model of the toolholder is BT30. In order to carry out the impact test, a PCB force hammer was used to excite the motorized spindle at the tip of the tool and test rod, and the accelerometer was installed on the tip of the tool and rod. The experiment setup is shown in Fig. 7. The results of the amplitude-frequency response comparison between the experiment and simulation as shown in Fig. 8. The results predicted by the model are in good agreement at the first modal. Because the machining error, thread, sleeve, and other details of the spindle are not considered in modeling, the other natural vibration frequencies are not entirely consistent. Still, the prediction trend of the whole model is relatively consistent with the test results.

The stiffness of the motorized spindle is nonlinear with the load. In order to further verify the correctness of the model, the motorized spindle is loaded statically in Fig. 9. The loading position is 175mm extended from the spindle interface, and the measuring position is 90mm and 230mm from the interface. In order to eliminate the error caused by the displacement of the fixed device, one of the displacement sensors measures the displacement of the motorized spindle housing. Loaded the motorized spindle from 0 to 2000N, and the results are shown in Fig. 10. The displacement result of motorized spindle under constant stiffness is linear. In practice, the experiment indicates the displacement either in 90mm or 230mm positions is nonlinear, where the change rate decreases with the increase of the load. Therefore, the variable stiffness model considering the nonlinearity is closer to the experimental results.

5 Model analysis and discussion

To illustrate the feasibility and effectiveness of the proposed method, a case example is given to analyze a certain motorized spindle in the machining center. In the spindle structure, the bearing from front to back is bearing 1, bearing 2, bearing 3, bearing 4. The rotating speeds of the two working conditions are 4000r/min and 2500r/min, respectively. The acquisition equipment with a Kistler dynamometer brand collected cutting forces, as shown in Fig. 11 and Fig. 12.
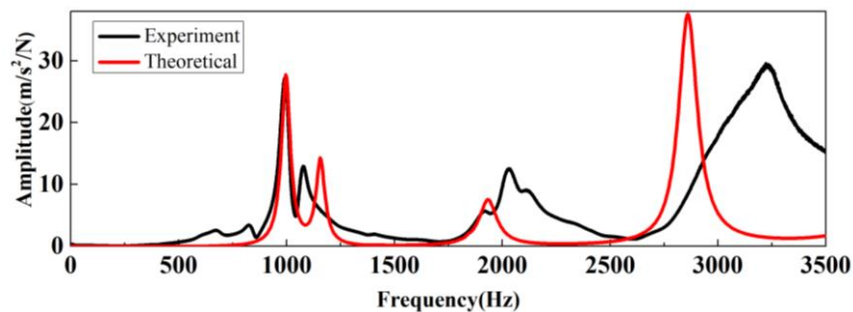

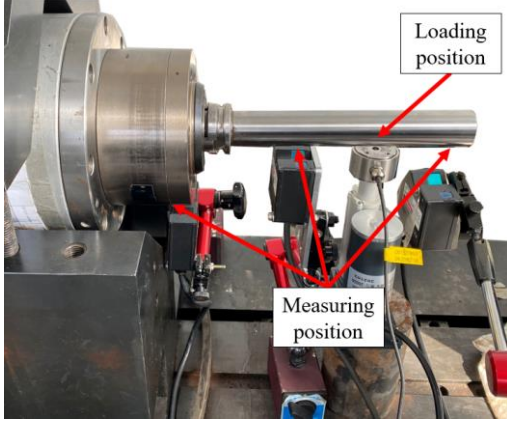Fig. 8 Prediction results of tooltip dynamics

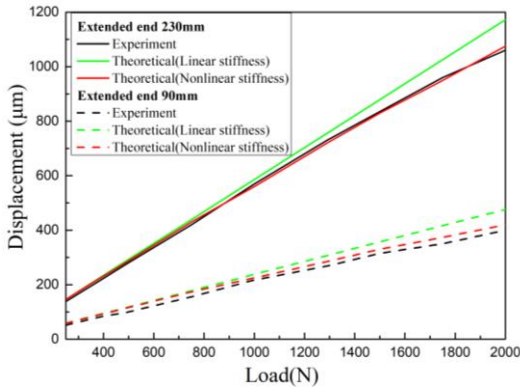Fig. 9 Experimental of the loading for motorized spindle

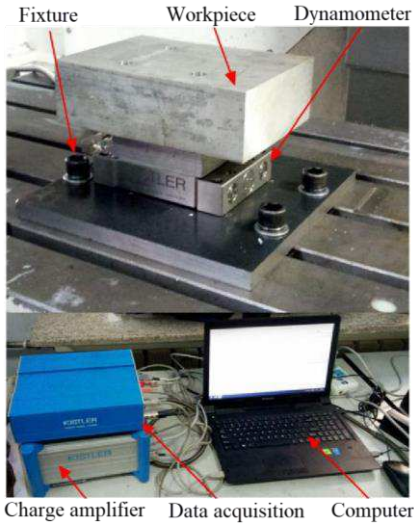Fig. 10 Displacement of motorized spindle under load

Fig. 11 Acquisition of the cutting force

5.1 Influence of preload and cutting force on bearing lifetime

The preload is the initial axial load on the bearings for the motorized spindle to obtain high stiffness and increase rotational. The preload has a great impact on spindle stiffness, rotating precision, and service lifetime.
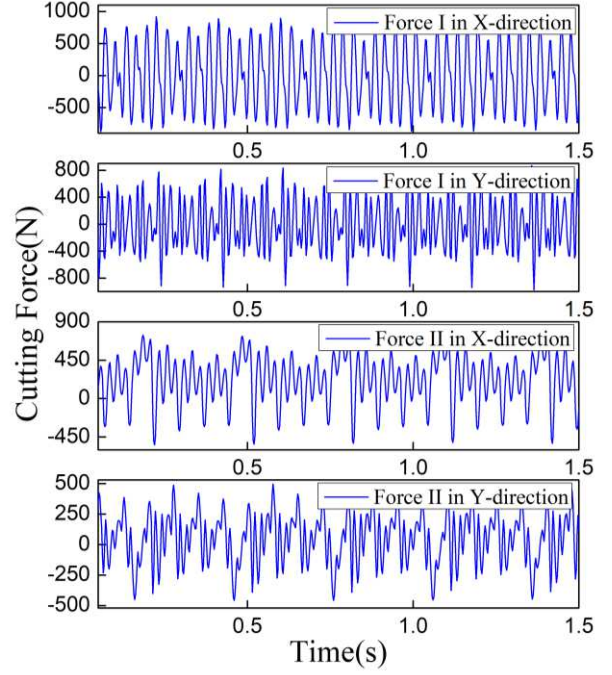
8

Fig. 12 Cutting force of CNC

For analyzing the preload for the lifetime, the filtering of the cutting force data, the obtained cutting force I, and cutting force II are brought into Eq.(1) as the excitation load {F}. The average effective load Pm on each bearing in the motorized spindle is obtained according to Eq.(12). The loads on each bearing under the cutting force are shown in Fig. 13. In order to analyze the bearing load more accurately, the influence of preload on bearing load is eliminated. The bearing 1 at the front end of the motorized spindle bears the most load, and the load increases gradually by the increase of preload. This phenomenon is possible due to the stiffness of the front bearing increases, the displacement of the shaft behind the bearing support position is restrained, that the rear bearing will bear less load. However, when the preload reaches a threshold value, the load on bearing 2 increases gradually. This phenomenon may be the front end bearing is closer to the rigid support, which increases the gyroscopic moment effect of the spindle and the deformation of bearing 2. The rear bearings are not sensitive to the increase of stiffness and almost unchanged, which is only affected by the overall cutting force level. By converting the measured cutting forces, the average values of the two cutting forces are 684N and 449N, respectively. The ratio of the two cutting forces is

1.5 times, but the load on the bearing 1 is not in this proportion, and the ratio of the load to cutting force of the front axle is increasing with the increase of rigidity. Therefore, the effect of cutting force on motorized spindle bearing is not linear.

The effect of the preload on the bearing load is shown in Fig. 14. Convert the preload into the load of the bearing, and the bearing load increase by the preload. When the preload is low, the load on the front bearing 2 decreases due to bearing 1 bears more cutting force with the increased stiffness. Due to the other bearing loads are small, the preload gradually dominates the bearing loads, and the load increases linearly with the increase of the preload.

Fig. 15 shows the lifetime of the bearings and the bearing group lifetime in the motorized spindle under the cutting force. Because the position at the front end is equivalent to a cantilever beam, the front bearing 1 is subjected to the most load and has the lowest lifetime. Due to the support of bearing 1, the load of bearing 2 decreases sharply, so the lifetime

of bearing 2 will be very long. As the preload gradually becomes dominant in the load on the bearing, the bearing lifetime will first increase and then decrease with preload. Still, the lifetime of the bearing group represented by the bearing group will continue to decline. The lifetime curve shapes under different cutting forces are proportional.

5.2 Influence of clamping force on bearing lifetime

Fig. 16 shows the influence of the different clamping forces on spindle vibration displacement amplitude under the cutting force I. The preload of each bearing is 280N. With the increase of the clamping force, the contact stiffness between the cone surface of the toolholder and the shaft increases, and the contact between them become closer, improving the spindle's stability under the cutting force and the vibration displacement amplitude will be smaller. Fig. 17 shows the lifetime of the bearings under the clamping force. With the
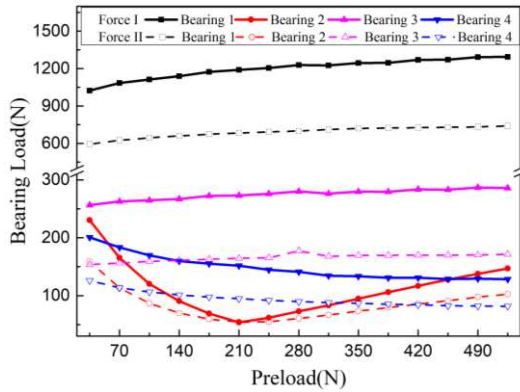

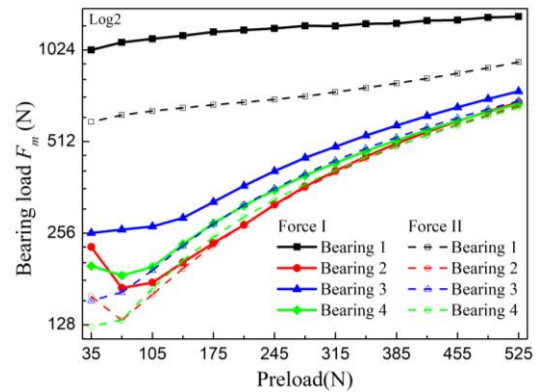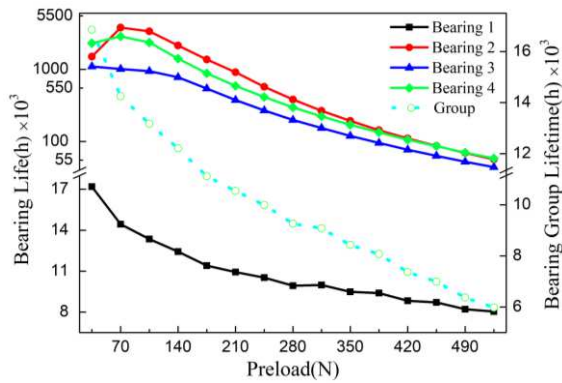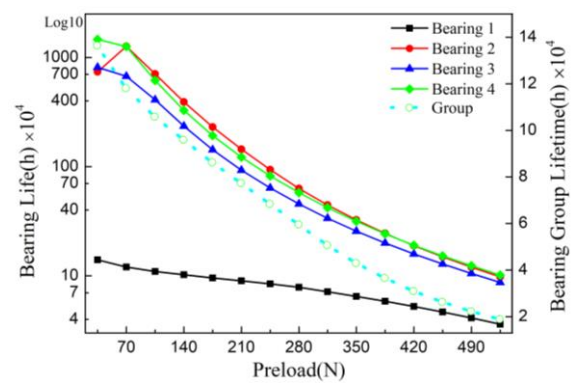Fig. 13 Bearing loads with different cutting force and preload

Fig. 14 The comparison of the bearing loads

(a)Cutting force I

(b) Cutting force II

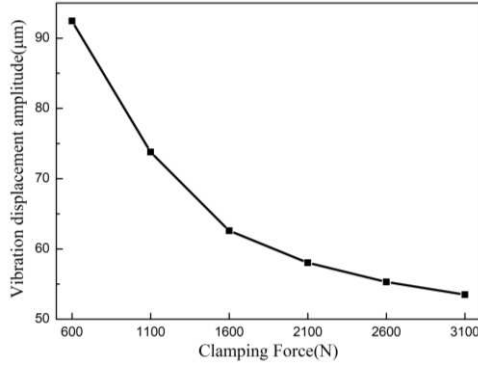Fig. 15 The comparison of the bearings lifetime.

9

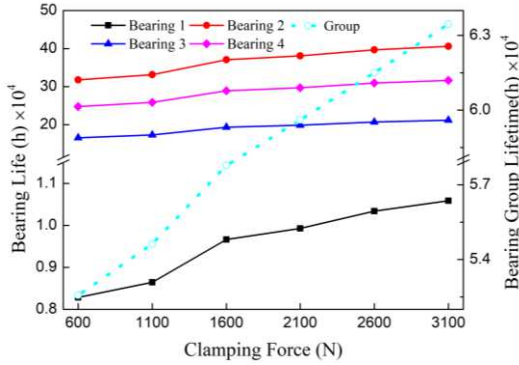Fig. 16 Vibration displacement amplitude with different contact stiffness

Fig. 17 The comparison of clamping force on lifetime

increase of the clamping force, the supporting stiffness of the toolholder increases, which reduces the inertial force caused by the bending of the toolholder under the cutting force when the motorized spindle rotates. Therefore, the lifetime of the front bearing 1 increases with the increased clamping force, and the lifetimes of other bearings also increase slightly. Hence, the lifetime of the motorized spindle increases significantly.

6 Conclusion

This paper studies a nonlinear dynamic spindle model to evaluate the lifetime of the motorized spindle bearings considering the dynamic cutting force.

The main conclusions of this paper are shown as follows.

(1) The nonlinear dynamic model of the motorized spindle is established. The measured cutting force is used as the dynamic model's input force to obtain the time history load on each bearing in the motorized spindle. Then, the time history load is converted into the average load by cycle counting,

introduced into the well-known bearing life model. Follow this, the lifetime of each bearing and its group are estimated. This method can reflect the load on the motorized spindle bearings in actual working conditions and provide a better lifetime estimation result for the motorized spindle in the design stage.

(2) The dynamic stiffness of the contact surface is established. The contact pressure distribution on the contact surface under radial and axial forces is analyzed and verified by the finite element model. Following this, the change of contact stiffness under two kinds of the load is deduced. The results show that the contact stiffness is linearly proportional to radial and axial forces. In addition, the validity of the whole dynamic model is verified by the impact test and loading test on the spindle. The test results indicate the proposed dynamic model calculates bearing load accurately.

(3) The influence of preload and broach force on bearing life is analyzed. The lifetime of the bearing group is mainly determined by the frontest bearing 1, which bears the heaviest load. The load on the bearing 2 can be affected by the front bearing stiffness, exhibiting the first decrease and then increase trend. The lifetime of the rear bearing is generally determined by the overall level of cutting force. When the load on the bearing is small, the bearing lifetime is mainly affected by the preload. With the increase of clamping force, the contact stiffness climbs, and the lifetime of the bearing group can be improved.

(4) Due to the nonlinear stiffness of each bearing, the load on each bearing does not increase linearly with the cutting force. According to the bearing lifetime model, the relationship between bearing load and bearing life is cubic. Therefore, considering the nonlinear stiffness of the motorized spindle dynamic model gives a better understanding of the relationship between cutting force and bearing load, providing a more realistic accurate result of bearing group lifetime.

Declarations

Conflicts of interest

Not applicable

Availability of data and material

Not applicable

Code availability

Not applicable

Authors' contributions

Jun Ying: Background research, Methodology, Data curation, Software, Validation Writing -original draft, Editing.
Zhaojun Yang: Supervision, Project administration, Funding acquisition
Chuanhai Chen: Review & editing, Supervision.
Guoxiang Yao: Assist in experiment, Data curation, Software.
Wei Hu & Hailong Tian: Modification suggestion

Ethics approval

Not applicable

Consent to participate

Not applicable

Consent for publication

Not applicable

Reference

[1] Baur M, Albertelli P, Monno M(2020) A review of prognostics and health management of machine tools. Int J Adv Manuf Technol 107: 2843–2863. https://doi.org/10.1007/s00170-020-05202-3.

[2] Patil RB, Kothavale BS, Waghmode LY(2019) Selection of time-to-failure model for computerized numerical control turning center based on the assessment of trends in maintenance data. P I MECH ENG O-J RIS 233(2): 105-117. https://doi.org/10.1177/1748006X18759124

[3] Cao H, Zhang X, Chen X (2017) The concept and progress of intelligent spindles: A review. Int J Mach Tools Manuf 112:21–52. https://doi.org/10.1016/j.ijmachtools.2016.10.005.

[4] Ritou M, Rabréau C, Le Loch S, et al (2018) Influence of spindle condition on the dynamic behavior. CIRP Ann 67:419–422. https://doi.org/10.1016/j.cirp.2018.03.007.

[5] Lv Y, Li C, Jin Y, et al (2021) Energy saving design of the spindle of CNC lathe by structural optimization. Int J Adv Manuf Technol 114:541–562. https://doi.org/10.1007/s00170-021-06758-4.

[6] He X (2016) Recent development in reliability analysis of NC machine tools. Int J Adv Manuf Technol 85:115–131. https://doi.org/10.1007/s00170-015-7926-0.

[7] Yang Z, Kan Y, Chen F, et al (2015) Bayesian reliability modeling and assessment solution for NC machine tools under small-sample data. Chinese J Mech Eng 28:1229–1239. https://doi.org/10.3901/CJME.2015.0707.088.

[8] Peng C, Cai Y, Liu G, Liao TW (2020) Developing a Reliability Model of CNC System under Limited Sample Data Based on Multisource Information Fusion. Math Probl Eng 2020:1–10. https://doi.org/10.1155/2020/3645858.

[9] Yang Z, Li X, Chen C, et al (2019) Reliability assessment of the spindle systems with a competing risk model. Proc Inst Mech Eng Part O J Risk Reliab 233:226–234. https://doi.org/10.1177/1748006X18770343.

[10] Mu Z, Zhang G, Ran Y, et al (2019) A reliability statistical evaluation method of CNC machine tools considering the mission and load profile. IEEE Access 7:115594–115602. https://doi.org/10.1109/ACCESS.2019.2935622.

[11] Peng W, Li Y, Yang Y, et al (2017) Bayesian Degradation Analysis With Inverse Gaussian Process Models Under Time-Varying Degradation

Rates. IEEE Trans Reliab 66:84–96. https://doi.org/10.1109/TR.2016.2635149.

[12] Guo J, Huang HZ, Peng W, Zhou J (2019) Bayesian information fusion for degradation analysis of deteriorating products with individual heterogeneity. Proc Inst Mech Eng Part O J Risk Reliab 233:615–622. https://doi.org/10.1177/1748006X18808964 2.

[13] Fu B, Zhao J, Li B, et al (2020) Fatigue reliability analysis of wind turbine tower under random wind load. Struct Saf 87:101982. https://doi.org/10.1016/j.strusafe.2020.101982.

[14] Nejad AR, Gao Z, Moan T (2014) On long-term fatigue damage and reliability analysis of gears under wind loads in offshore wind turbine drivetrains. Int J Fatigue 61:116–128. https://doi.org/10.1016/j.ijfatigue.2013.11.023.

[15] Cheng Q, Qi B, Liu Z, et al (2019) An accuracy degradation analysis of ball screw mechanism considering time-varying motion and loading working conditions. Mech Mach Theory 134:1–23. https://doi.org/10.1016/j.mechmachtheory.2018.12.024.

[16] Li G, Wang S, He J, et al (2019) Compilation of load spectrum of machining center spindle and application in fatigue life prediction. J Mech Sci Technol 33:1603–1613. https://doi.org/10.1007/s12206-019-0312-3.

[17] Zhang Y, Zhang M, Wang Y, Xie L (2020) Fatigue life analysis of ball bearings and a shaft system considering the combined bearing preload and angular misalignment. Appl Sci 10:1–22. https://doi.org/10.3390/APP10082750 2.

[18] Nelson HD (1980) A finite rotating shaft element using Timoshenko beam theory, J Mech Design 102: 793-803. https://doi.org/10.1115/1.3254824

[19] Inman DJ. Engineering Vibration. 3th. Pearson Prentice Hall, 2008.

[20] Sakamoto H, Matsuda T, Shimizu S (2012) Effect of clamped toolholders on dynamic characteristics of spindle system of machining center. Int J Autom Technol 6:168–174. https://doi.org/10.20965/ijat.2012.p0168.

[21] Mehrpouya M, Graham E, Park SS (2013) FRF based joint dynamics modeling and identification.

Mech Syst Signal Process 39:265–279. https://doi.org/10.1016/j.ymssp.2013.03.022.

[22] Özşahin O, Budak E, Özgüven HN (2015) In-process tool point FRF identification under operational conditions using inverse stability solution. Int J Mach Tools Manuf 89:64–73. https://doi.org/10.1016/j.ijmachtools.2014.09.014.

[23] Yang Y, Wan M, Ma YC, Zhang WH (2018) A new method using double distributed joint interface model for three-dimensional dynamics prediction of spindle-holder-tool system. Int J Adv Manuf Technol 95:2729–2745. https://doi.org/10.1007/s00170-017-1394-7.

[24] Cao Y, Altintas Y (2004) A general method for the modeling of spindle-bearing systems. J Mech Des Trans ASME 126:1089–1104. https://doi.org/10.1115/1.1802311

[25] Yoshimura M. Computer-aided design improvement of machine tool structure incorporatin joint dynamic data. Ann Cirp 1979; 28(1): 241-246.

[26] Xu C, Zhang J, Feng P, et al (2014) Characteristics of stiffness and contact stress distribution of a spindle-holder taper joint under clamping and centrifugal forces. Int J Mach Tools Manuf 82–83:21–28. https://doi.org/10.1016/j.ijmachtools.2014.03.006.

[27] Liu J, Ma C, Wang S, et al (2019) Contact stiffness of spindle-tool holder based on fractal theory and multi-scale contact mechanics model. Mech Syst Signal Process 119:363–379. https://doi.org/10.1016/j.ymssp.2018.09.037.

[28] Naderi M, Iyyer N (2015) Fatigue life prediction of cracked attachment lugs using XFEM. Int J Fatigue 77:186–193. https://doi.org/10.1016/j.ijfatigue.2015.02.021.

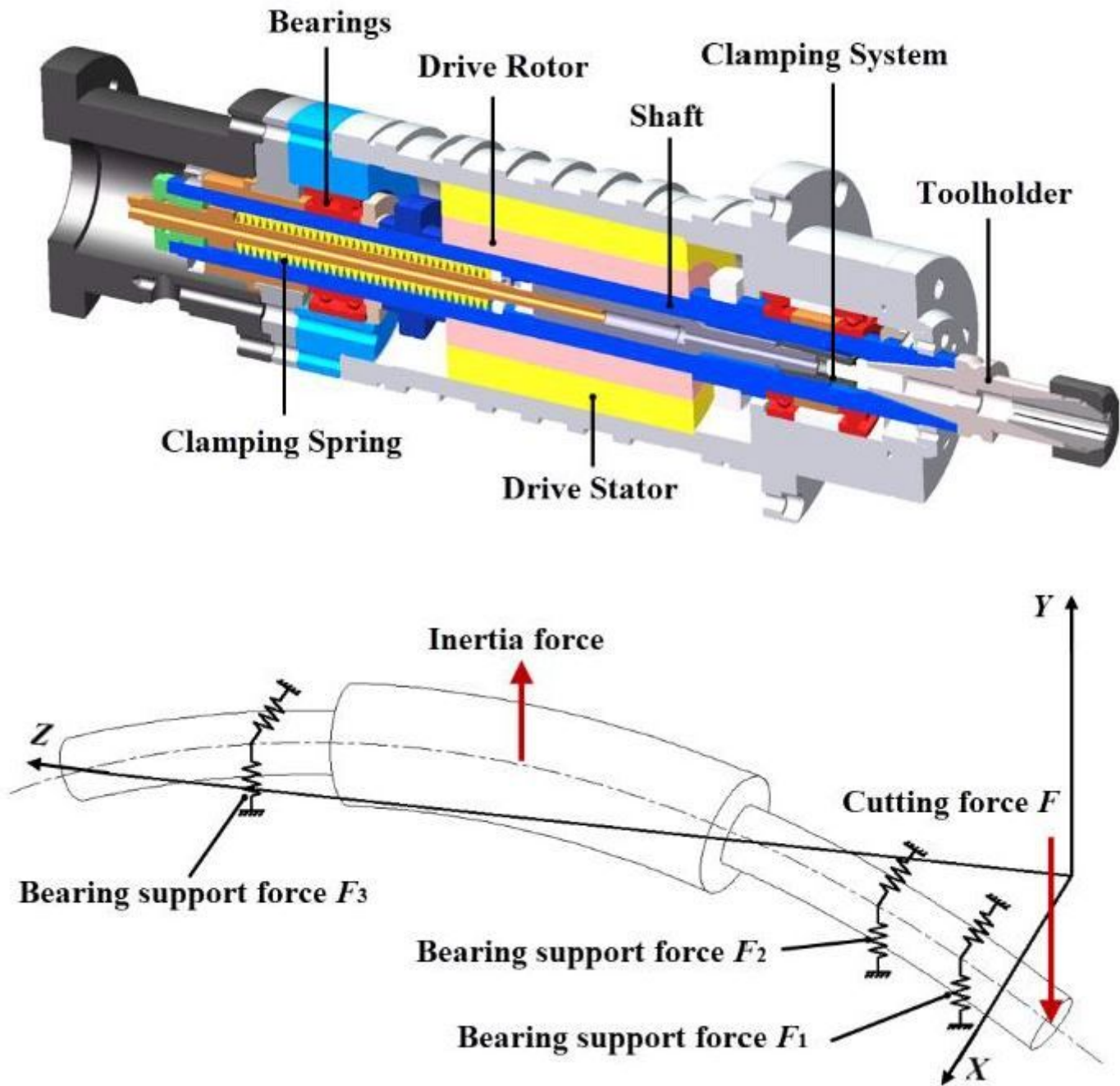[29] Yakout M, Elkhatib A, Nassef MGA (2018) Rolling element bearings absolute life prediction using modal analysis. J Mech Sci Technol 32:91–99. https://doi.org/10.1007/s12206-017-1210-1.

Figures

Figure 1

The motorized spindle system

Shaft

Tool

- Node ——— Beam Element
- Translational stiffness and damping in Z direction
- Translational stiffness and damping in X direction
- Angular stiffness and damping around Z-axis
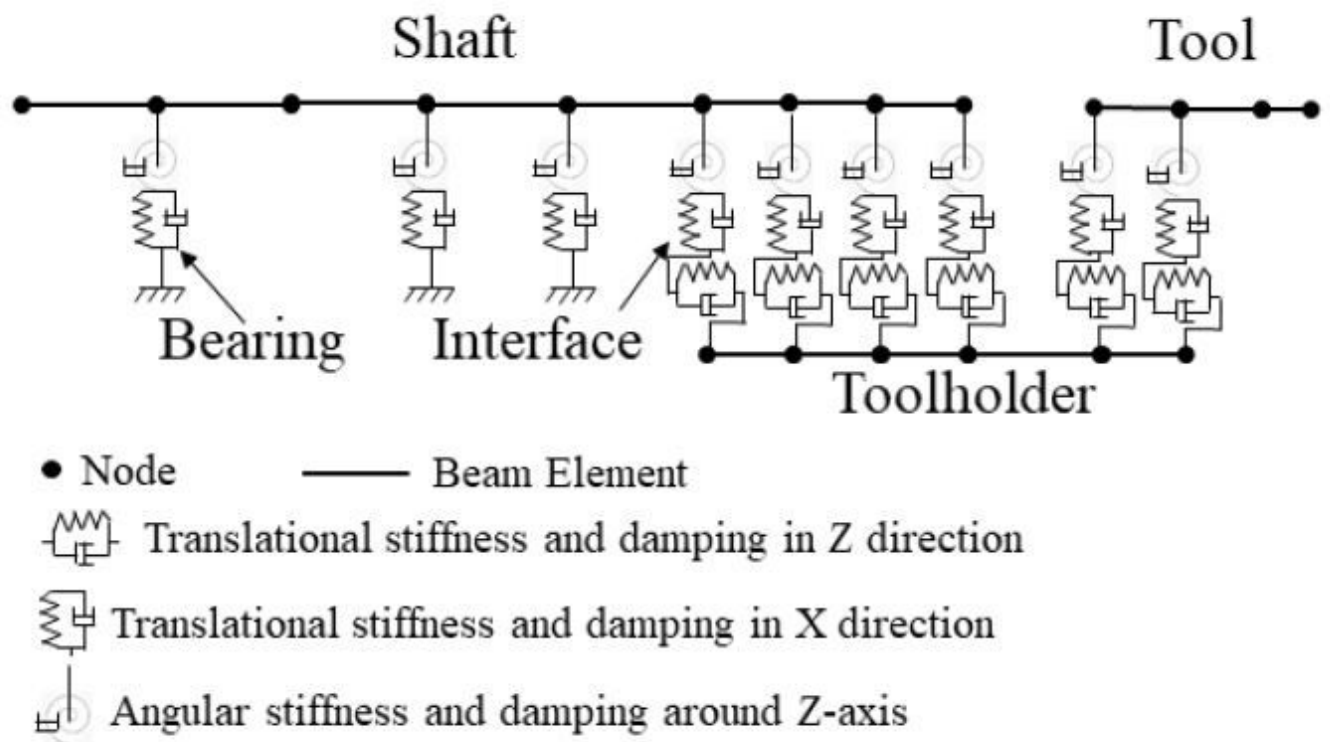
Bearing   Interface

Toolholder

Figure 2

Finite element model for the spindle-bearing system
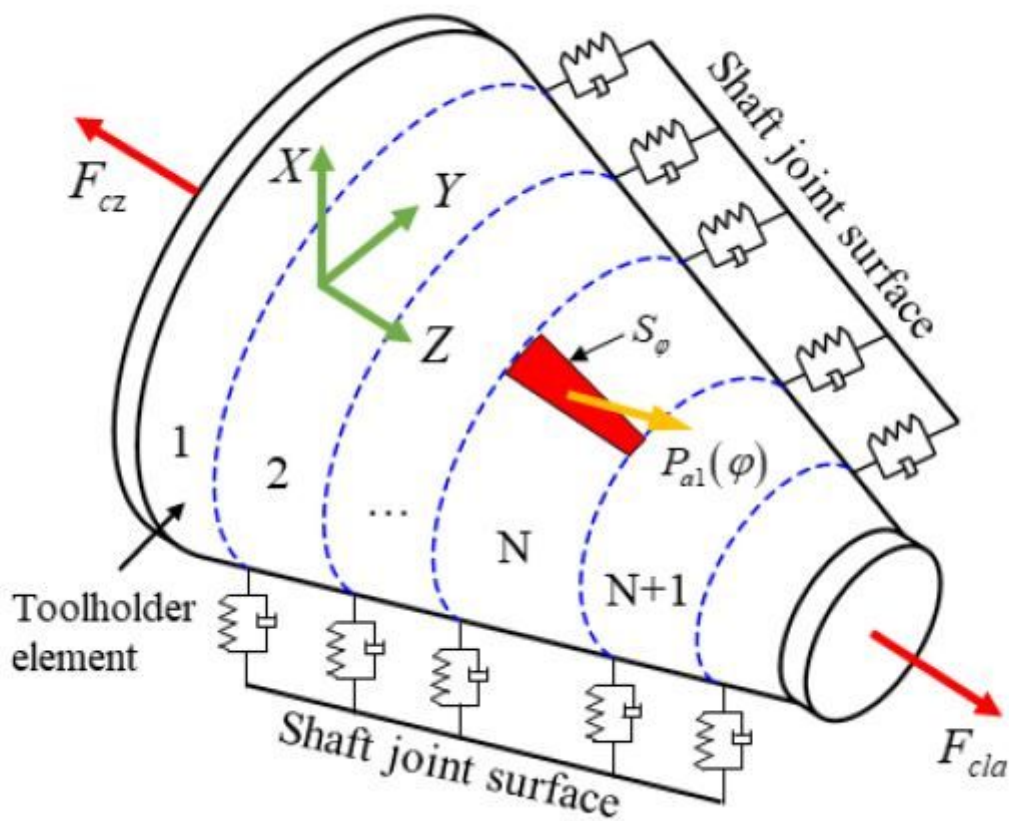
Figure 3
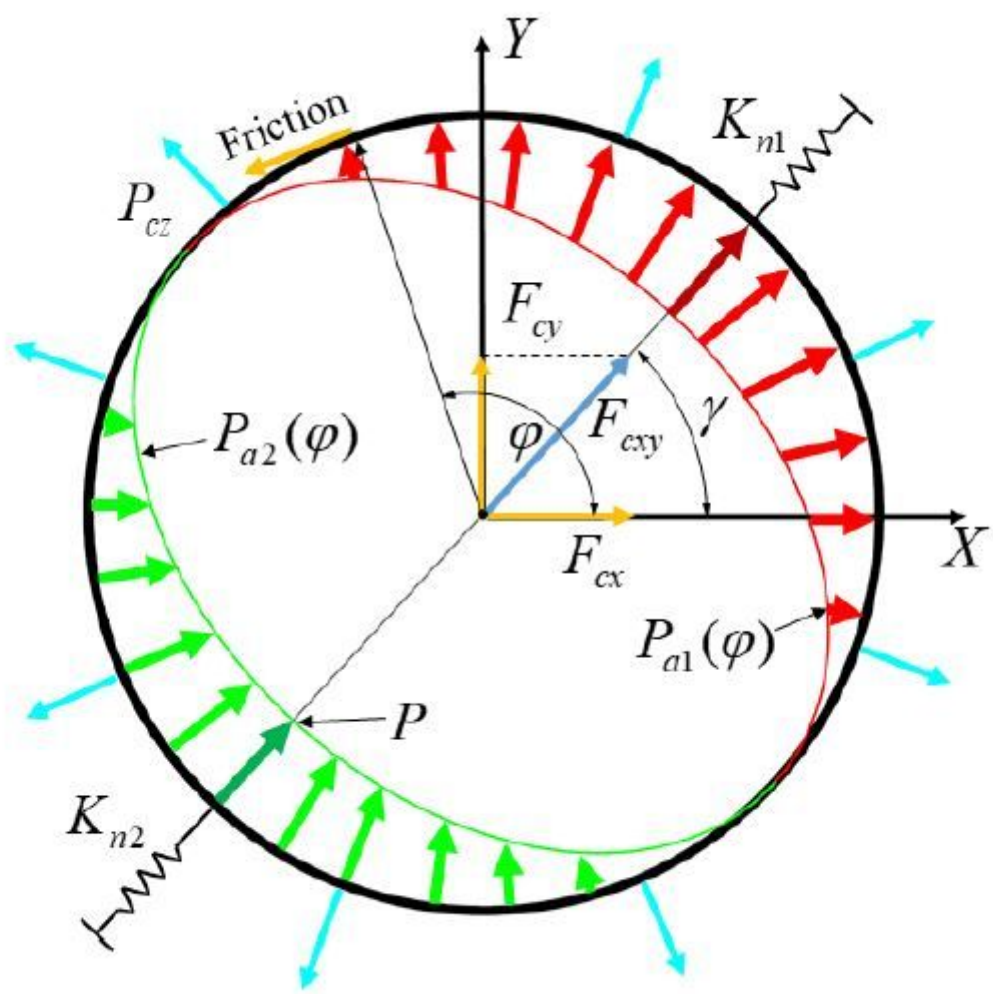
The model of toolholder under clamping and axial force
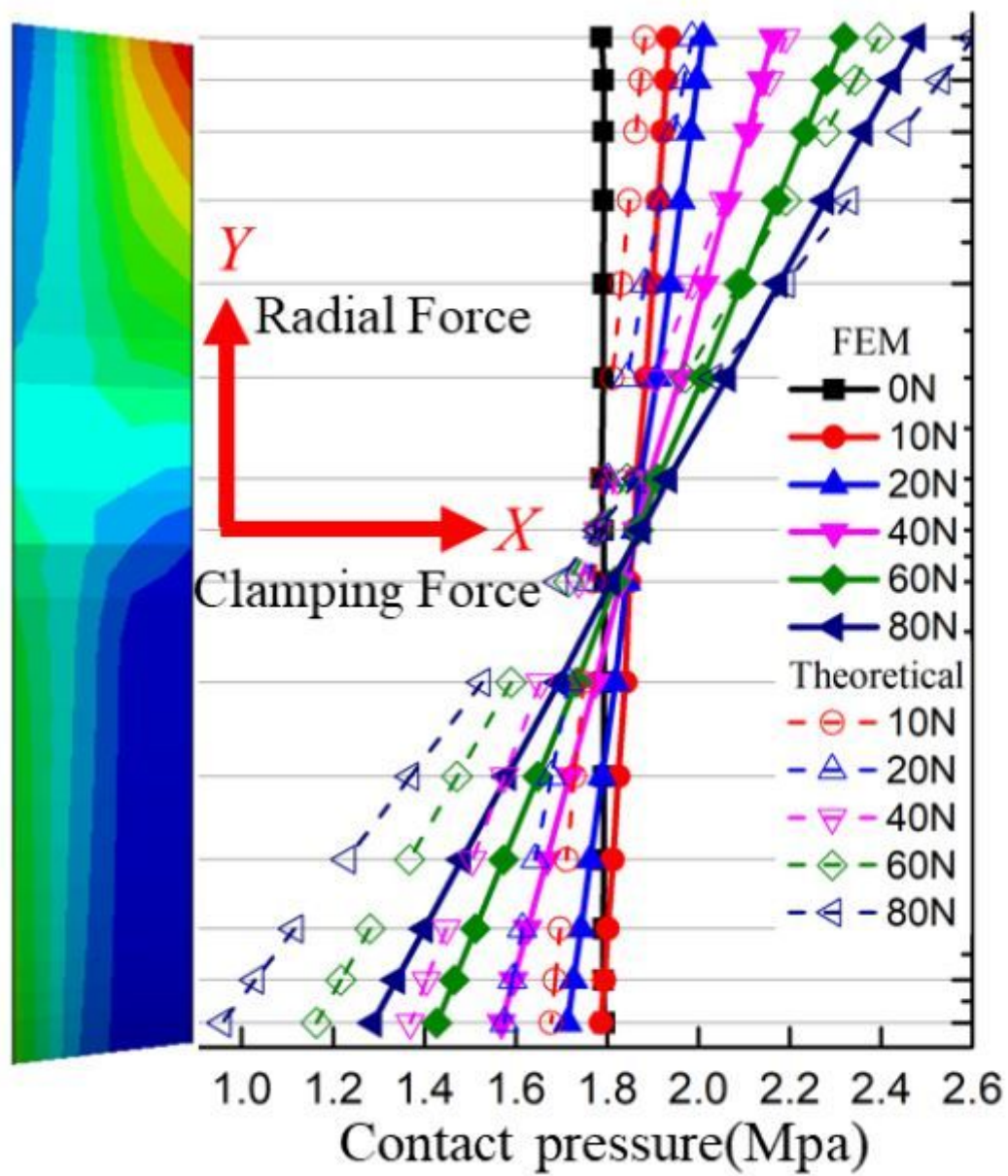

Figure 4

Force analysis of the element under the radial force

Figure 5

The contact pressure distribution of toolholder unit
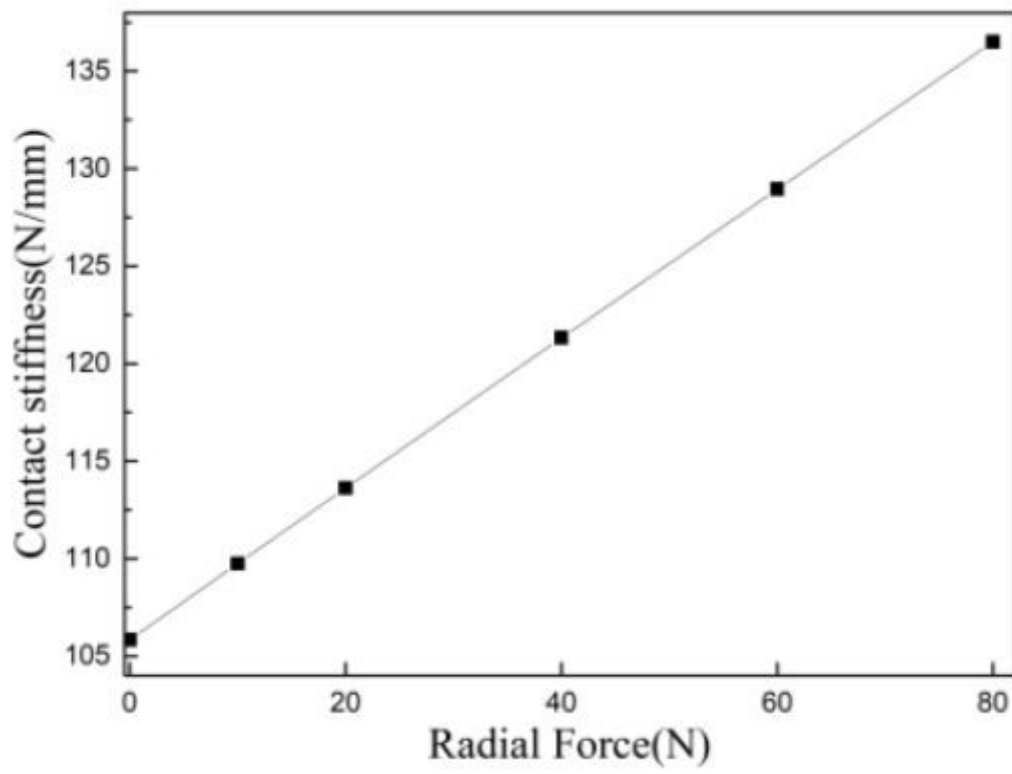
Figure 6

Contact stiffness under radial force
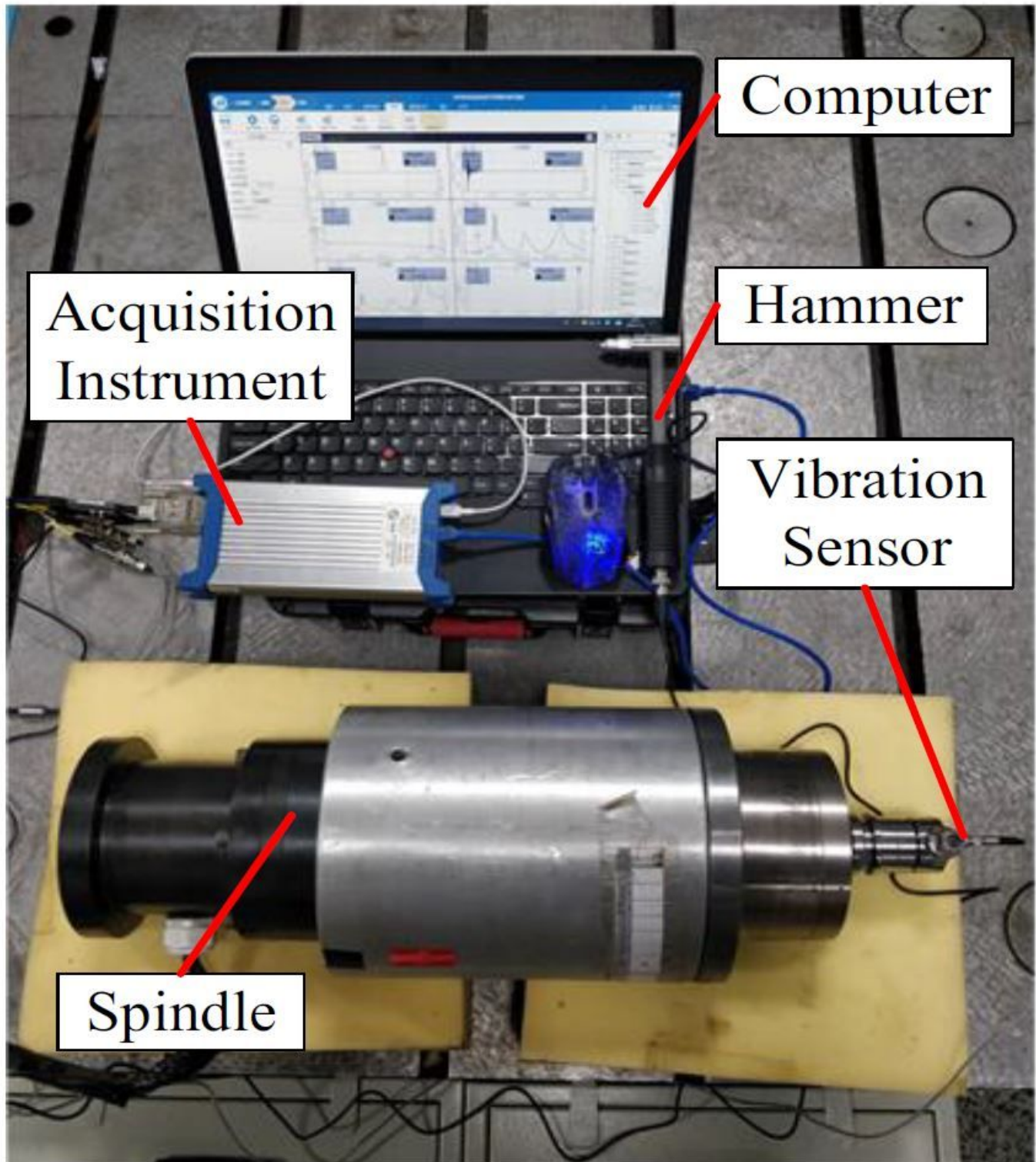
Figure 7

Experimental setup for the spindle
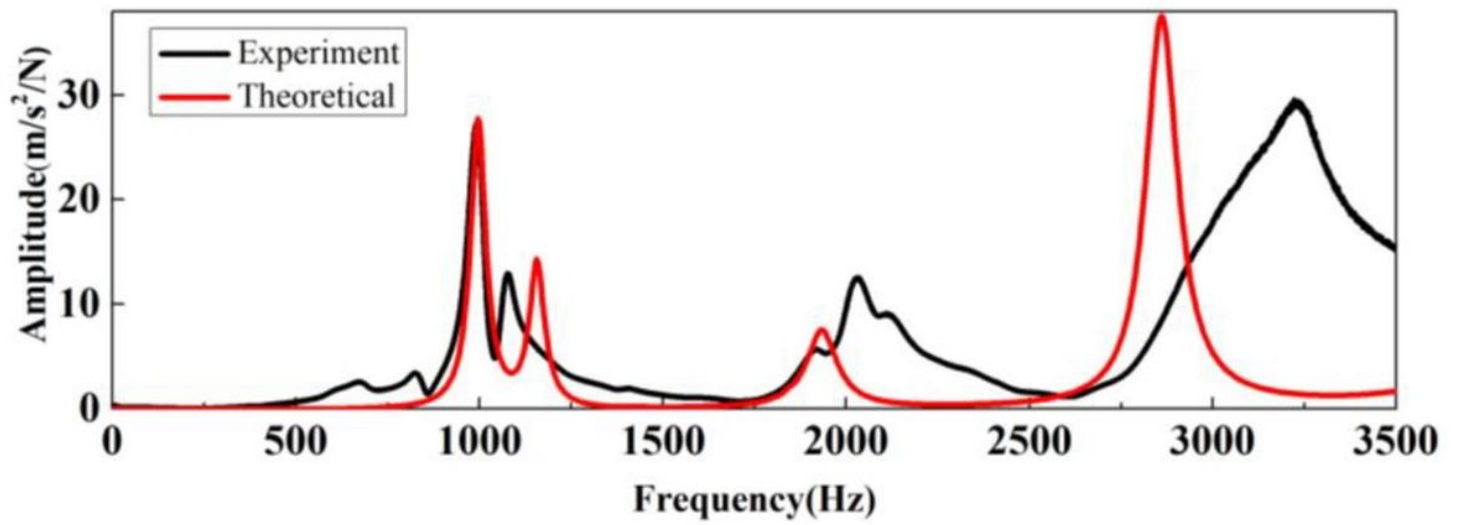
Figure 8

Prediction results of tooltip dynamics
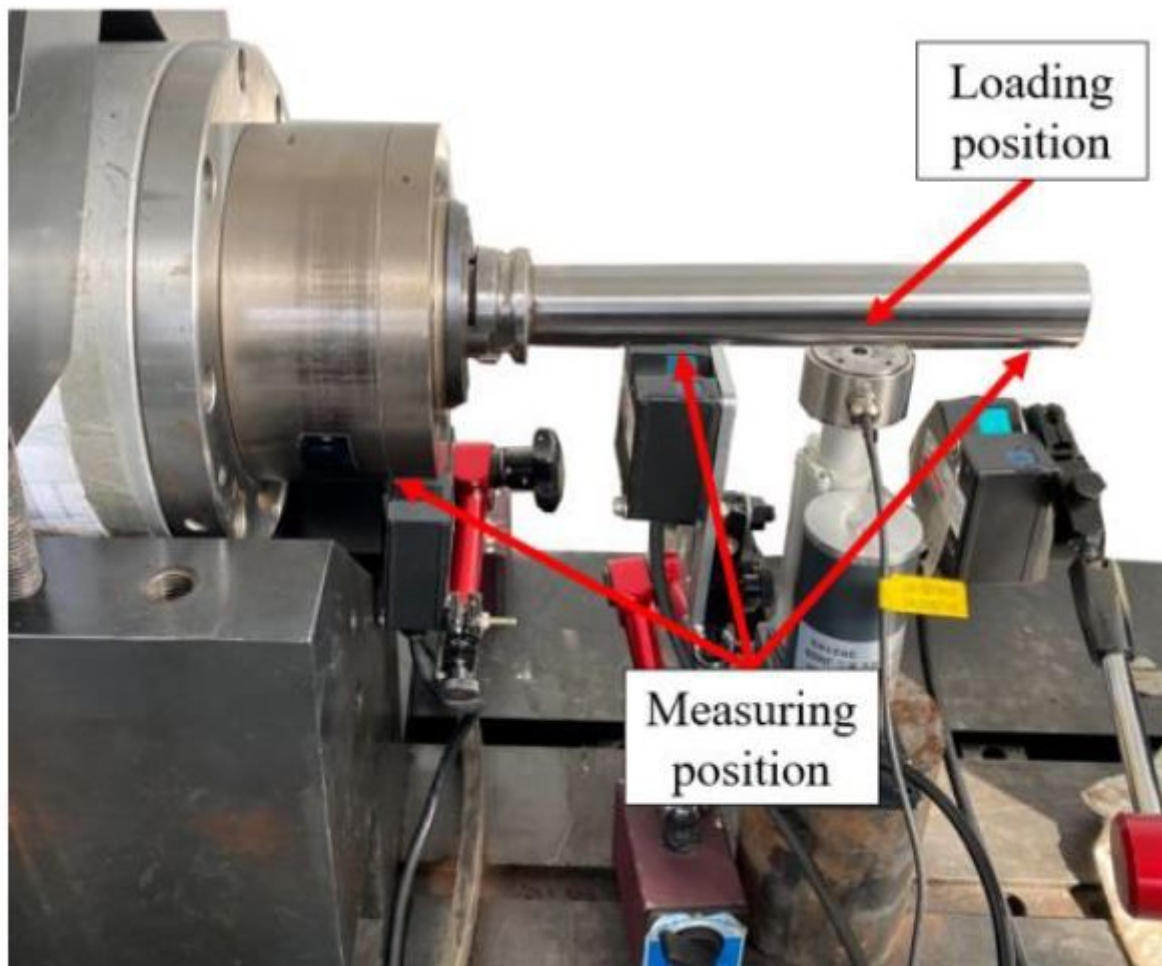
Figure 9

Experimental of the loading for motorized spindle
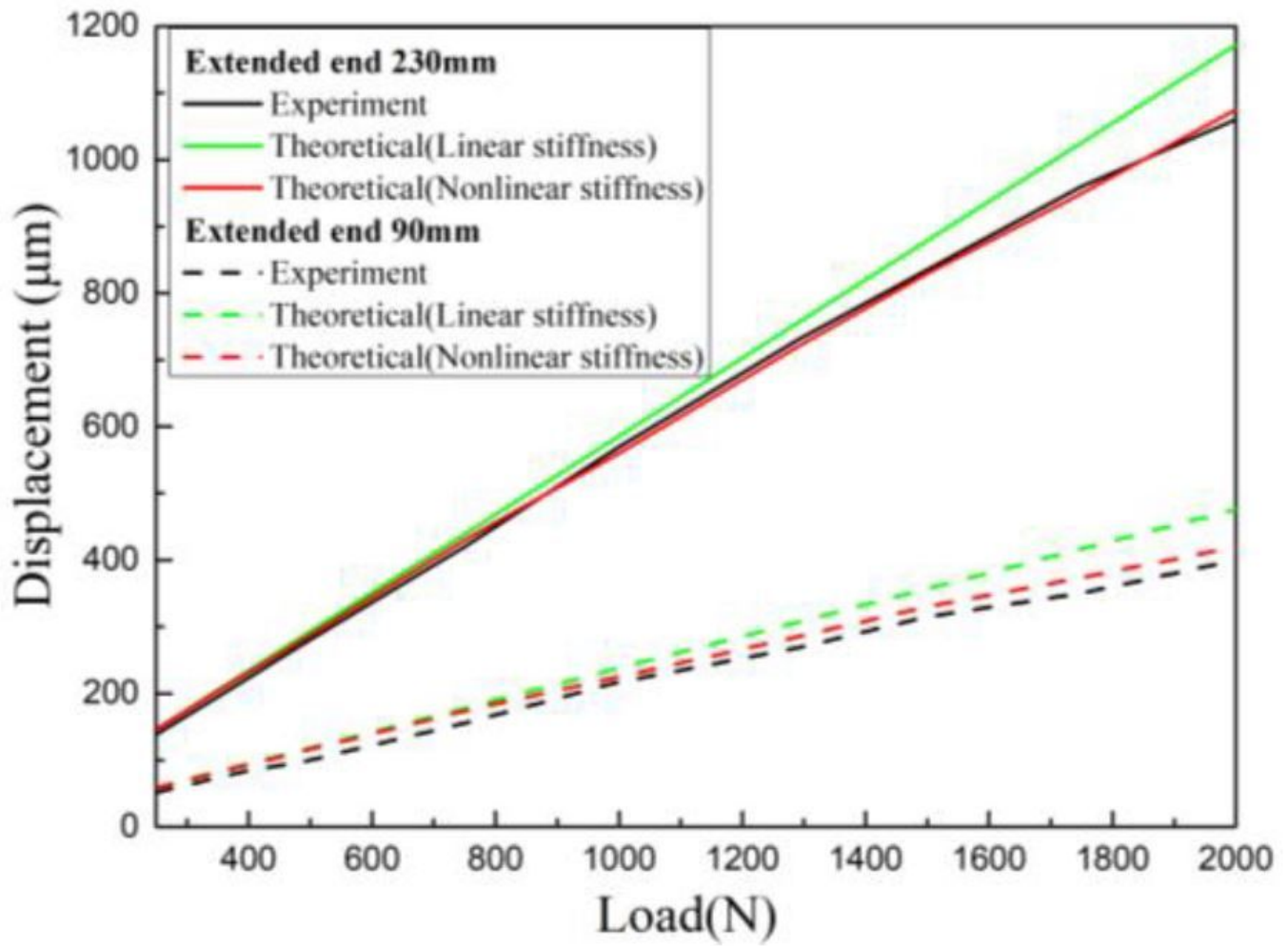
Figure 10

Displacement of motorized spindle under load
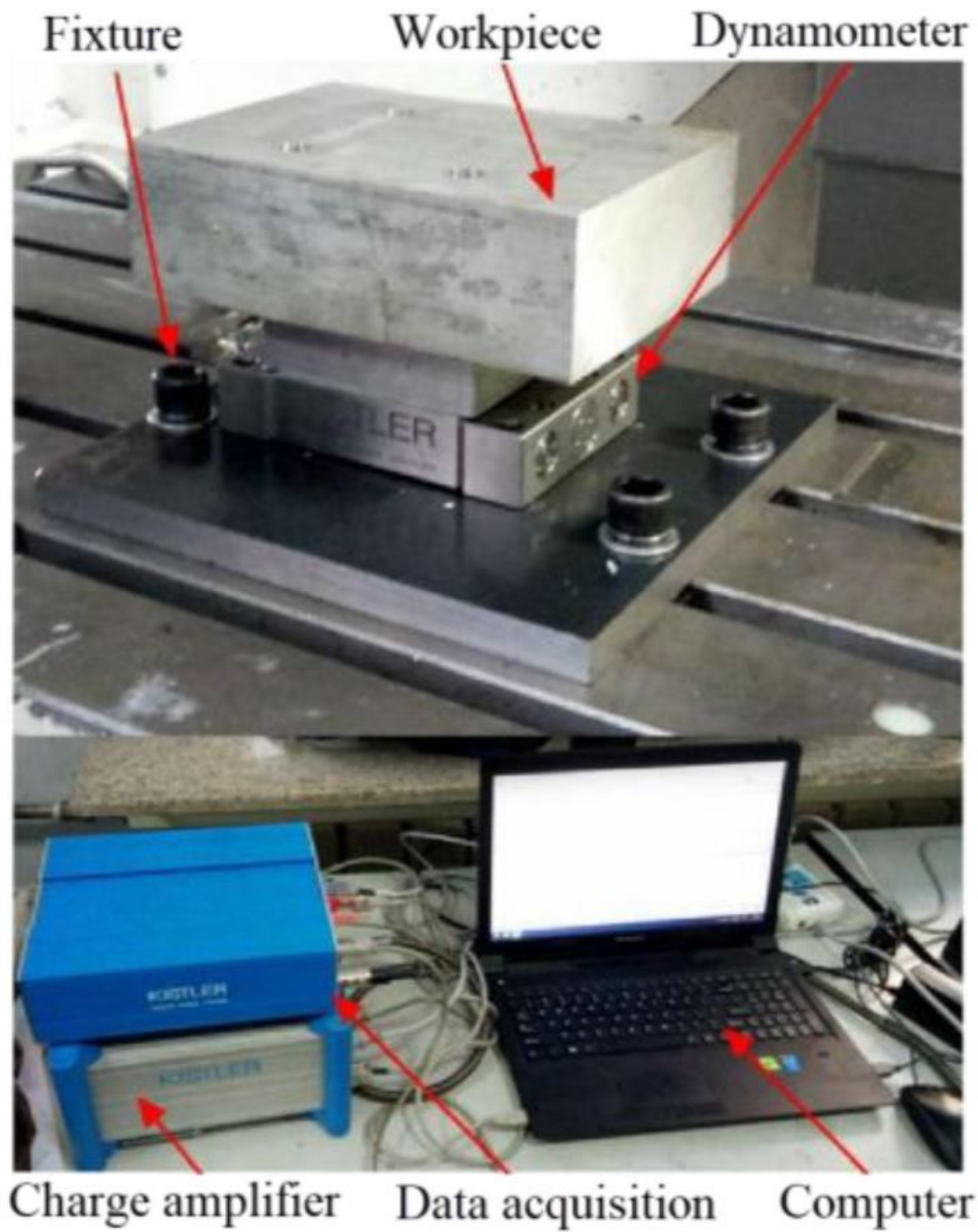
Figure 11

Acquisition of the cutting force
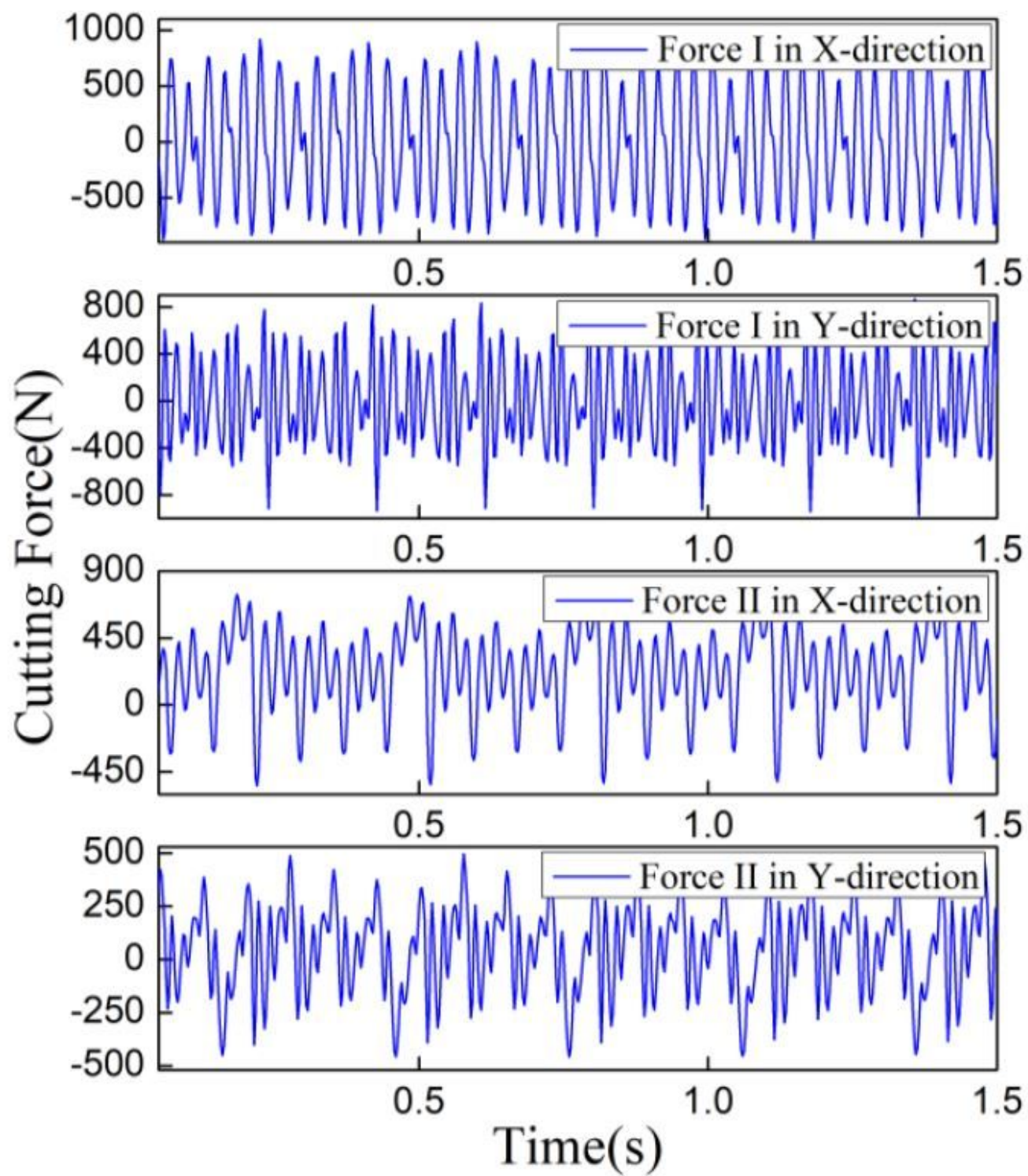
Figure 12

Cutting force of CNC
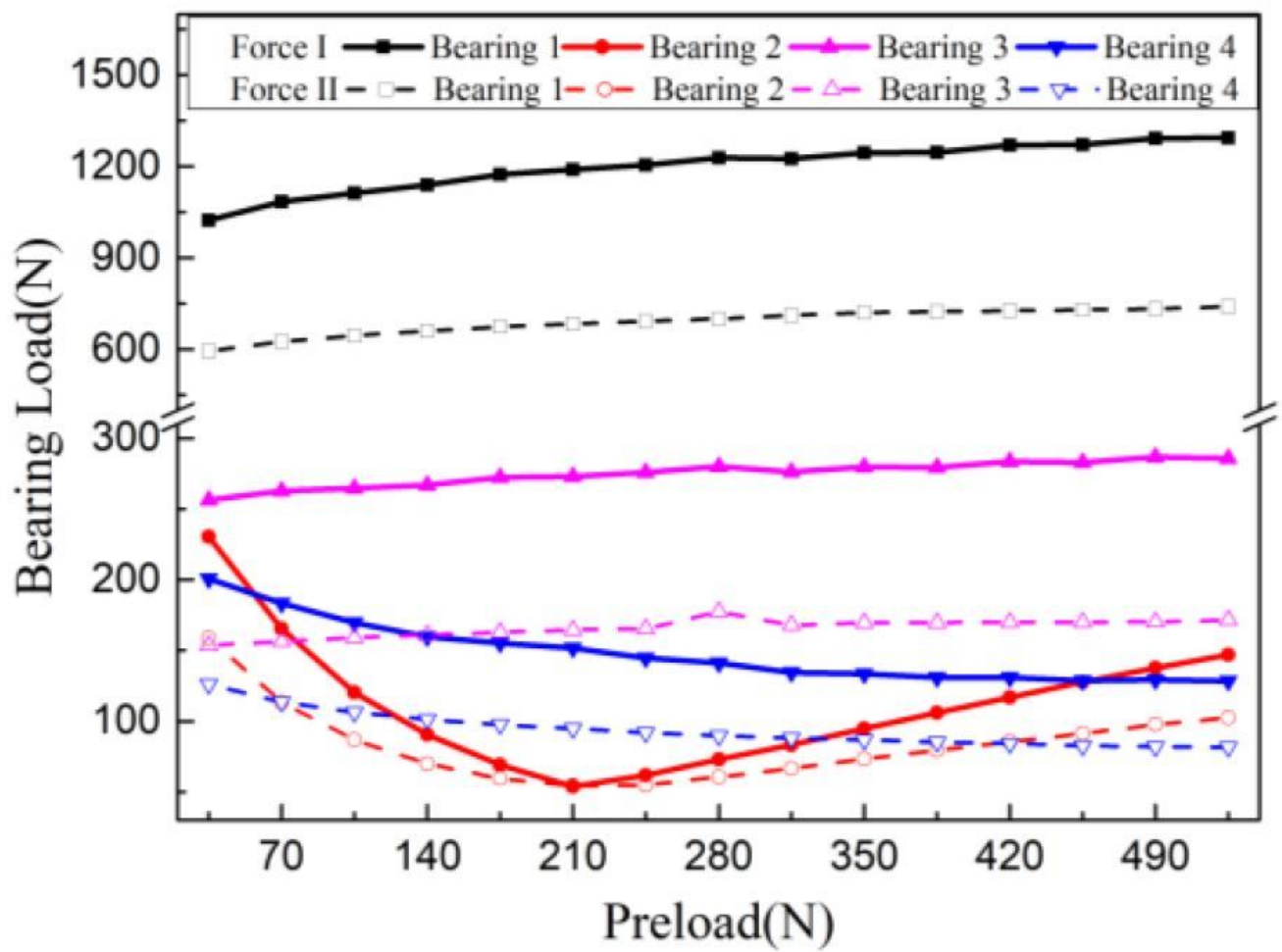
Figure 13
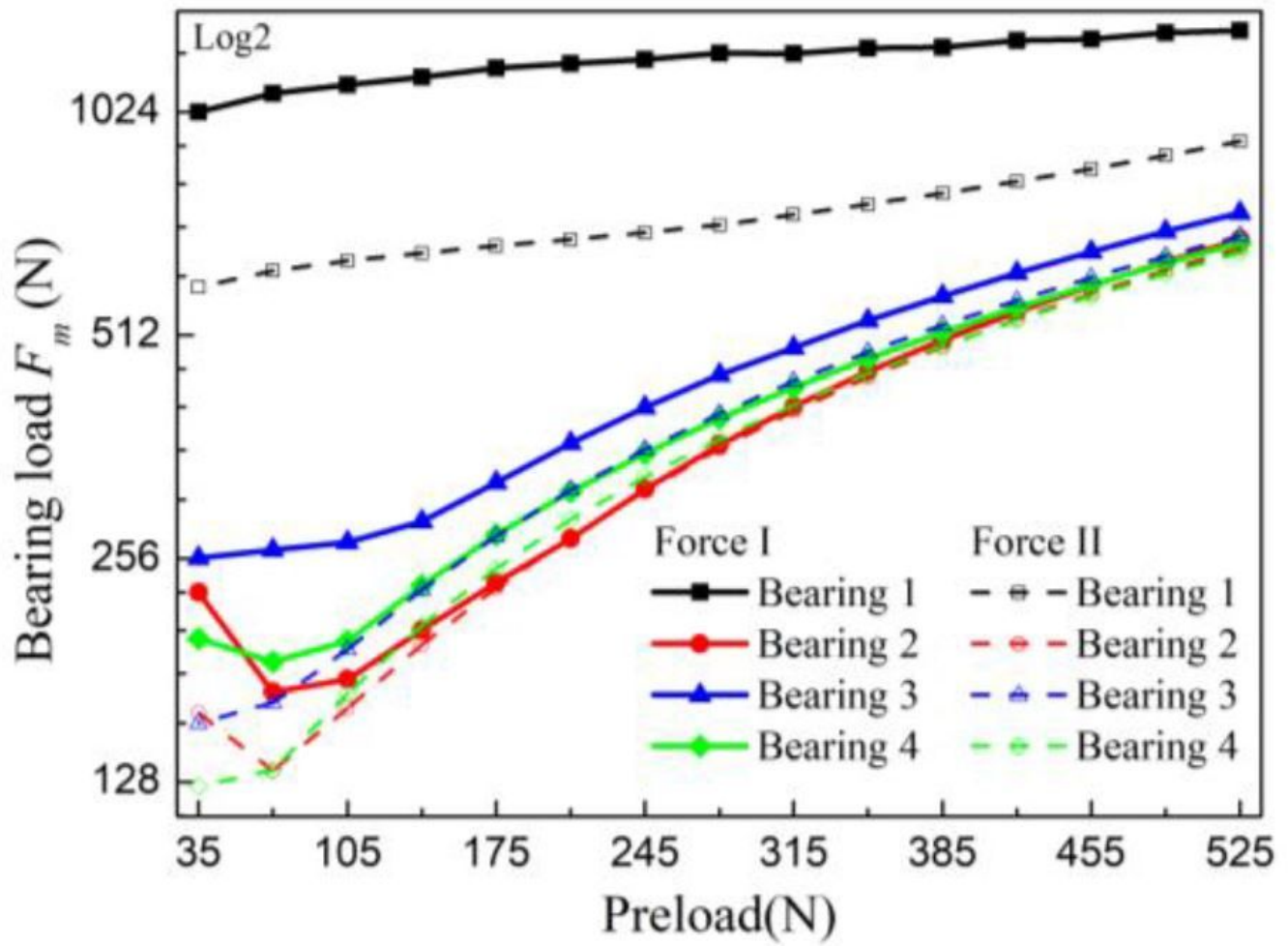
Bearing loads with different cutting force and preload
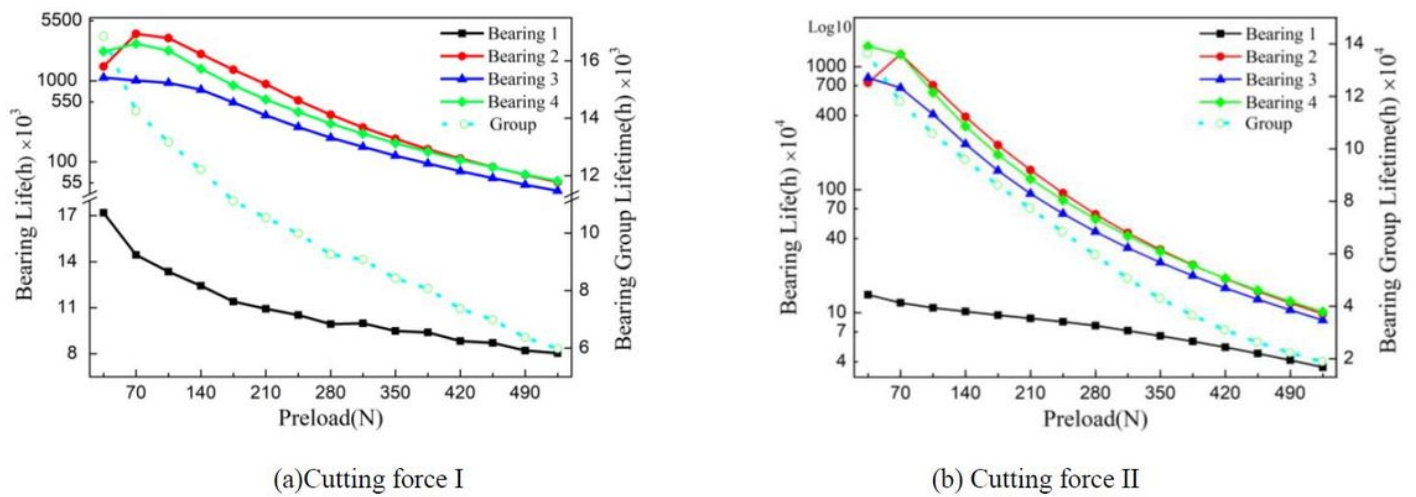
Figure 14

The comparison of the bearing loads

(a)Cutting force I

(b) Cutting force II

Figure 15
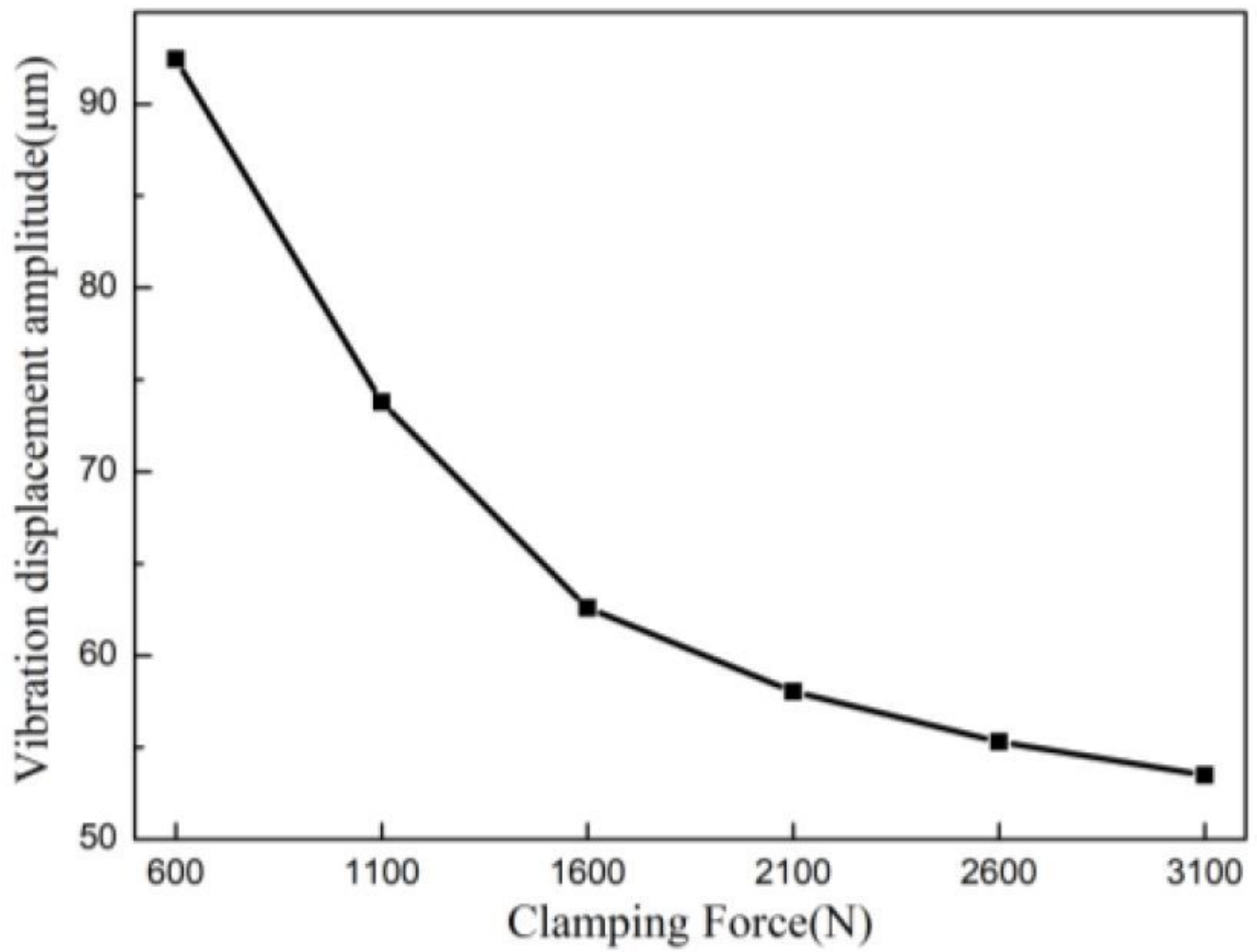
The comparison of the bearings lifetime.

Figure 16

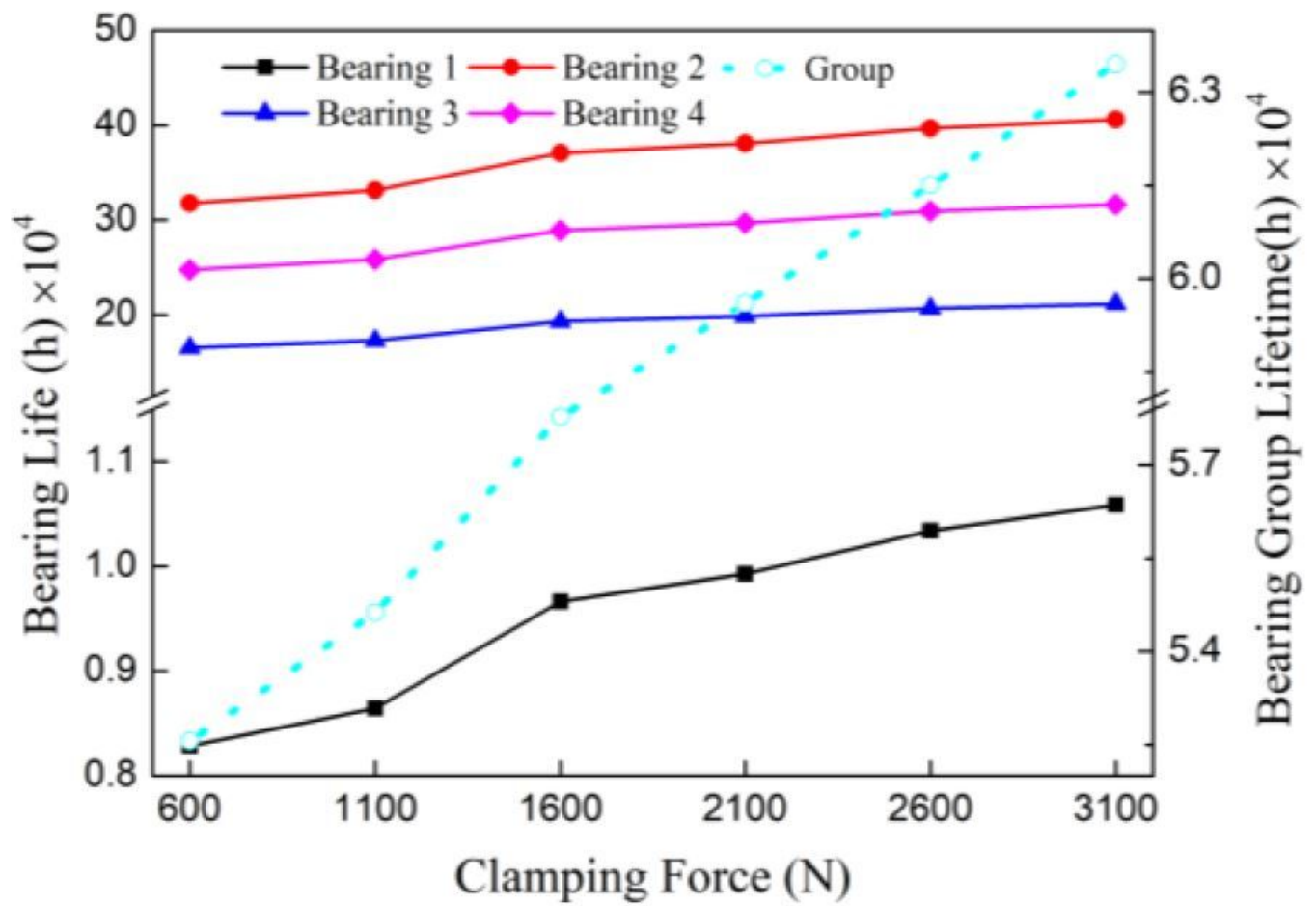Vibration displacement amplitude with different contact stiffness

Figure 17

The comparison of clamping force on lifetime